Biogeosciences

Modeling pCO_2 Variability in the Gulf of Mexico

Zuo (George) Xue[1, 2, &3], Ruoying He[4], Katja Fennel[5], Wei-Jun Cai[6], Steven Lohrenz[7], Wen-Jen Huang[8]， Hanqin Tian[9,] Wei Ren[10]

1. Dept. of Oceanography and Coastal Sciences, Louisiana State University, Baton Rouge, LA, United States
2. Center for Computation and Technology, Louisiana State University, Baton Rouge, LA, United States
3. Coastal Studies Institute, Louisiana State University, Baton Rouge, LA, United States
4. Dept. of Marine, Earth & Atmospheric Sciences, North Carolina State University, Raleigh, NC, United States
5. Dept. of Oceanography, Dalhousie University, Halifax, Canada
6. School of Marine Science and Policy, University of Delaware, Newark, DE, United States
7. School for Marine Science and Technology, University of Massachusetts Dartmouth, New Bedford, MA, United States
8. Department of Oceanography, National Sun Yat-sen University, Kaohsiung, Taiwan
9. School of Forestry and Wildlife Sciences, Auburn University, AL, United States
10. Department of Plant and Soil Sciences, University of Kentucky, Lexington, KY, United States

Abstract

A three-dimensional coupled physical-biogeochemical model was used to simulate and quantify temporal and spatial variability of sea surface pCO_2 in the Gulf of Mexico (GoM). The model was driven by realistic atmospheric forcing, open boundary conditions from a data-assimilative global ocean circulation model, and observed freshwater and terrestrial nutrient and carbon input from major rivers. A seven-year model hindcast (2004–2010) was performed and validated against ship measurements. Model results revealed clear seasonality in surface pCO_2 and were used to compute carbon budgets in the Gulf. On average, the GoM was found to be a CO_2 sink with a flux of 1.11×10^{12} mol C yr^{-1}, which, together with the enormous fluvial carbon input, was balanced by the carbon export through the Loop Current. Two sensitivity model experiments were performed: one without biological sources and sinks and the other using river input from the 1904-1910 period as simulated by the Dynamic Terrestrial Ecosystem Model (DLEM). It was found that biological uptake was the primary driver making GoM an overall CO_2 sink and that the sub-regional carbon budget was susceptible to changes in river forcing. When the 1904-1910 river conditions were applied, the northern GoM became a CO_2 source instead.

1. Introduction

Human consumption of fossil fuels has resulted in continuously increasing levels of atmospheric CO_2 since the Industrial Revolution began around 1750. If the increasing trend continues, the projected pCO_2 by the end of the 21st century (970 ppm, in A1F1 scenario, Stocker et al., 2014) could be nearly triple the present level. In face of different climate scenarios, a better understanding of the oceans' role in regulating the global carbon cycle is crucial, because oceans not only act as receivers of the enormous carbon loading from coastal rivers (Cai el al., 2011a; Bauer et al. 2013), but also as vast carbon reservoirs via the "carbon pump" mechanism (Sabine et al., 2004; Sabine and Tanhua, 2010). On regional scales, the marine carbon cycle tends to be more complicated and shows contrasting behaviors in different areas (coastal vs. open ocean, low latitude vs. high latitude, etc.) and during different seasons (e.g., Lohrenz et al., 2010 for the northern Gulf of Mexico; Jiang et al., 2008 for the South Atlantic Bight; Signorini et al., 2013 for the North American east coast; Tsunogai et al., 1999 for the East China Sea). Quantifying the ocean carbon budget is therefore a difficult task. Coupled physical and biological models are useful tools for understanding complex biogeochemical processes and estimating carbon and nutrient fluxes in coastal oceans where spatial and temporal heterogeneities are high and data are sparse (e.g. Fennel and Wilkin, 2009; Fennel 2010; Fennel et al., 2011; and He et al., 2011).

Our study focuses on the carbon cycle in the Gulf of Mexico (GoM). One unique feature of the gulf environment is that it receives enormous riverine nutrient and carbon inputs, the majority of which are from the Mississippi-Atchafalaya River system. Excessive nutrient and carbon loading causes coastal eutrophication, which triggers not

63 only the well-known hypoxia phenomenon (a.k.a. the "Dead Zone", Rabalais et al., 2002),
64 but also a newly revealed coastal ocean acidification problem (Cai et al, 2011b).
65 However, the carbon budget associated with such enormous terrestrial carbon and
66 nutrient inputs remains unclear: on the one hand extensive riverine carbon input results in
67 CO_2 over-saturation in coastal waters, which serve as a CO_2 source to the atmosphere (e.g.
68 Lohrenz et al., 2010; Guo et al., 2012); on the other hand, although the Mississippi River
69 Plume region is an overall heterotrophic system that breaks down organic carbon
70 (Murrell et al., 2013), enhanced primary production in the river plume due to significant
71 inputs of inorganic nutrients induce a net influx of CO_2. Further offshore, the circulation
72 in the GoM is largely influenced by the energetic Loop Current. Large anticyclonic
73 eddies aperiodically pinch off from the Loop Current (Sturges and Leben, 2000), which,
74 along with the wind-driven cross-shelf circulation and other meso-scale and sub-
75 mesoscale processes, enhance material exchanges between the eutrophic coastal waters
76 and oligotrophic deep-ocean waters (e.g., Toner et al., 2003). Indeed, a recent
77 observational study suggested a significant dissolved inorganic carbon export (DIC, ~
78 3.30×10^{12} mol C yr^{-1}) from the GoM shelves to the Loop Current waters (Wang et al.,
79 2013).

80 While global inorganic carbon budgets have been made available through joint
81 seawater CO_2 observations (e.g. World Ocean Circulation Experiment and Joint Global
82 Ocean Flux study, Sabine et al., 2004; Feely et al., 2004; Orr et al., 2005), they are too
83 coarse to represent CO_2 variability in the GoM (Gledhill et al., 2008). Other recent efforts
84 were able to provide GoM sub-regional carbon assessments based on limited in situ
85 observations (e.g. Cai et al., 2003, Lohrenz et al., 2010, Huang et al., 2013, 2015a and

86 2015b focused on the Mississippi River plume and the Louisiana Shelf; Wang et al., 2013
87 covered three cross-shelf transects in the northeastern GoM but only for one summer).
88 Significant uncertainties exist in such budget estimations due to large temporal and
89 spatial gaps presented in the observations (e.g. Coble et al., 2010; Hofmann et al., 2011;
90 Robbins et al., 2014). In this regard, coupled physical-biogeochemical models are
91 capable of representing the biogeochemical cycle with realistic physical settings (e.g.,
92 ocean mixing and advection) and providing an alternative means for a gulf-wide carbon
93 budget assessment.

94 Here we present a GoM pCO_2 analysis based on the results of a coupled physical-
95 biogeochemical model simulation. Our objective is to quantify the pCO_2 flux at the air-
96 sea interface (which at present is based on observational analyses alone and subject to
97 large uncertainty), as well as its variability in relationship with river plume dynamics and
98 dominant oceanic processes in different regions of the GoM.

99

100 **2. Method**

101 Our analysis uses solutions from a coupled physical-biogeochemical model
102 covering the GoM and South Atlantic Bight waters (Xue et al., 2013, model domain see
103 Fig.1). The circulation component of the coupled model is the Regional Ocean Modeling
104 System (ROMS, Haidvogel et al. 2008, Shchepetkin and McWilliams, 2005; Hyun and
105 He, 2010) and is coupled with the biogeochemical module described in Fennel et al.
106 (2006, 2008, and 2011). A seven-year (January 1, 2004–December 31, 2010) model
107 hindcast was performed, driven by realistic atmospheric forcing (North America
108 Regional Reanalysis, www.cdc.noaa.gov), open boundary conditions from a data-

assimilative global ocean circulation model (HYCOM/NCODA, Chassignet et al., 2007), and observed freshwater and terrestrial nutrient input from 63 major rivers (Aulenbach et al., 2007; Milliman and Farnsworth, 2011; Fuentes-Yaco et al., 2001; and Nixon, 1996). Model validations (physics, nutrients and chlorophyll) and a nitrogen budget have been reported in Xue et al. (2013).

In this study we focus on the carbon cycle in the GoM. As in Xue et al. (2013), we considered the first year of the simulation (2004) as model spin-up; all results presented here are for model output from 2005 to 2010. The carbonate chemistry of the coupled model is based on the standard defined by the Ocean Carbon Cycle Model Intercomparison Project Phase 2 (Orr et al., 2000). There are two active tracers, DIC and alkalinity, to determine the other four variables of the carbonate system (i.e. pCO_2, carbonate ion concentration, bicarbonate ion concentration, and pH; Zeebe and Wolf-Gladrow, 2001). Details of the formulas used in simulation are provided in the supplementary materials S1.

Similar to the results reported by Hofmann et al. (2011), we found the model-simulated DIC concentration in the water column were very sensitive to the initial conditions. Although there are many historical measurements in the GoM, these data are limited in the northern GoM shelf regions and thus are insufficient to initialize the model. Instead, we tested model sensitivity using three sets of initial and open boundary conditions, which were derived using the empirical salinity-temperature-DIC-alkalinity relationships described in Lee et al. (2000 and 2006), Cai et al. (2011a), and Wang et al. (2013), respectively. Among them, the initial condition prescribed following Lee et al. (2000 and 2006, Fig.2) provided the best model-data comparison. For the open boundary

condition, we found simulated surface pCO_2 exhibited very limited variance (<5%) regardless which conditions were applied. To be consistent with the setup of the initial condition, the results presented here were driven by boundary conditions derived from Lee et al., (2000 and 2006).

The carbon cycle parameterizations used in this study followed the same approach and values as in Fennel et al. (2008), Fennel and Wilkin (2009), and Fennel (2010). For gas exchange calculation we followed the formulas in Wanninkhof (1992, details see supplementary materials S2). For air pCO_2, we utilized the Atmospheric Infrared Sounder (AIRS, 2008) monthly gridded observation dataset and averaged them over the study area. We applied the curve-fitting method using a C language program named CCGCRV (http://www.esrl.noaa.gov/gmd/ccgg/mbl/crvfit/crvfit.html, Fig.3), and the air pCO_2 in the gas exchange calculation was prescribed as:

$$pCO_{2air} = D0+D1*t+D2*(t^2)+D3*\sin(pi2*t)+D4*\cos(pi2*t) + D5*\sin(pi2*2*t)+D6*\cos(pi2*2*t) \quad (1)$$

where pCO_{2air} represents the monthly air pCO_2; t represents the number of months since January 2004 divided by 12, $pi2$ is a constant set to 6.28, $D0$=375.96, $D1$=2.23, $D2$=-0.007, $D3$=1.31, $D4$=-0.64, $D5$= -0.13, $D6$=0.21, and $D7$=0.09. Due to the relative low horizontal resolution of the AIRS data (2.5*2 degree), air pCO_2 was set to be spatially uniform.

To account for riverine inputs, we constructed climatological monthly alkalinity time series by averaging all available U.S. Geological Survey (USGS) observations for each major river. Because direct riverine DIC measurements were not available, we

155 approximated riverine DIC inputs using the corresponding alkalinity value plus 50,
156 following Guo et al. (2012). The fluvial DIC input to the GoM was estimated as ~ 2.18 ×
157 10^{12} mol C yr^{-1}, the majority of which was delivered by the Mississippi-Atchafalaya
158 River (~ 1.80 × 10^{12} mol C yr^{-1}, Fig.4, comparable with the estimation in Cai et al., 2003).
159 The results of three model experiments covering the period of 2004-2010 are
160 presented in this study. Experiment 1 (Exp1): Control run, with observed riverine inputs
161 from USGS and biological sources and sinks of DIC and alkalinity in the water column;
162 Experiment 2 (Exp2): No-biology run, where all biological sources and sinks of DIC and
163 alkalinity were disabled, similar to the experiment described in Fennel and Wilkin (2009);
164 Experiment 3 (Exp3): the same set up as Exp1, but the riverine inputs (water, nutrients,
165 and carbon of the Mississippi-Atchafalaya river) were taken from the Dynamic Land
166 Ecosystem Model (DLEM, Tian et al., 2015) simulation for the period of 1904-1910 (Fig.
167 4). Also in Exp2 the air pCO_2 was set to the 1904-1910 condition derived by formula (1).
168 The purpose of Exp2 is to examine roles of biological processes in regulating regional
169 pCO_2 variability, whereas Exp3 is to connect variability of coastal carbon dynamics with
170 historical climate and land-use changes within the Mississippi watershed.
171
172 **3. Validation of the control run**
173 We utilized the ship-based sea surface pCO_2 database composed by the Lamont-
174 Doherty Earth Observatory (LDEO Version 2014, >180,000 data points in the Gulf over
175 2005-2010, Takahashi et al., 2015) and Huang et al. (2015a and b) for model validation
176 (see locations of ship measurements in Fig.5). The ship measurements by Huang et al.
177 (2015a and b) were taken in October 2005; April, June, August 2006; May, August 2007;

January, April, July, November 2009; and March 2010, respectively and contains > 78,000 data points. To alleviate the spatial and temporal mismatches associated with these in-situ measurements, we computed their temporal and spatial mean using a 10-day temporal window, and then compared them with model-simulated pCO_2 time series (Fig.6). To facilitate our analysis, the GoM was divided into five sub-regions: 1) Mexico Shelf (MX Shelf), 2) West Gulf of Mexico Shelf (WGoM Shelf), 3) Northern Gulf of Mexico Shelf (NGoM Shelf), 4) West Florida Shelf (WF Shelf), and 5) the open ocean, which is > 200m water depth (regional definitions followed Benway and Coble, 2014, maps of sub-regions see Fig.1).

On the NGoM Shelf, the model simulation was able to capture the measured pCO_2 in 21 out of the 26 data groups (the mean value of in-situ measurements fell in one standard deviation of the model mean). Specifically, agreement between model and observations was better during spring, fall, and winter, than during summer. The model overestimated pCO_2 in June 2006, August 2007, and July 2009. These discrepancies will be discussed in later sections. On the Gulf-wide scale, the control run reproduced the observed seasonality. Decent model-data agreements were found in 24 out of the 26 data groups. These sub-regional and Gulf-wide comparisons indicate that the coupled physical-biogeochemical model is generally capable of resolving temporal and spatial variations in observed pCO_2, allowing us to use this seven-year hindcast to further characterize the air-sea CO_2 flux.

4. Results

In this section, we present model-simulated sea surface pCO_2 and air-sea CO_2 flux in the five sub-regions. Because large pCO_2 gradients were found in both in-situ measurements and model in shallow waters, areas that are 10m deep and shallower were excluded from our analysis.

4.1 Temporal variability of Sea Surface pCO_2

Spatially averaged model-simulated pCO_2 on the NGoM Shelf exhibited clear seasonality, with large values (~ 500 ppm) around August and smallest values (~ 300 ppm) around February (Fig.6a). Notably, spatial averaged pCO_2 on the NGoM Shelf were not coincident with high river carbon and nutrient inputs (Fig.3). Simulated pCO_2 peaks were generally two to three months later than maximum river input in a year. The maximum riverine input during 2005-2010 was observed in June 2008 when a major flood occurred (Fig. 4a), yet no significant elevation of pCO_2 was seen in the model simulation. Gulf-wide spatially averaged pCO_2 (Fig.4b) had a temporal pattern similar to that on the NGoM Shelf, with high pCO_2 values (~ 425 ppm) in August and low values (~ 350 ppm) in February. Averaged pCO_2 on the NGoM Shelf was generally 50 ppm higher than that in the entire gulf.

4.2 Air-Sea CO_2 flux

The carbon flux was calculated based on a multi-year model mean (2005-2010). We found the GoM overall was a CO_2 sink with a mean flux rate of 0.71 mol C m^{-2} yr^{-1} (~ 1.11×10^{12} mol C yr^{-1}, Table 1 and Fig.7). Examining region by region, we found that

224 the open ocean, occupying ~ 65% of the GoM in area, acted as a CO_2 sink (1.04 mol m^{-2}
225 yr^{-1} of C) during most of the year except in summer. The greatest carbon uptake occurred
226 in winter (2.44 mol C m^{-2} yr^{-1}). It is evident that waters around the Loop Current act as a
227 sink throughout the year, whereas the western part of the open ocean waters shifted from
228 acting as a CO_2 source in summer and fall to a sink in winter and spring.

229 Compared with the open ocean, air-sea flux on the continental shelf was more
230 location-dependent and varied from season to season. Among the four shelf sub-regions,
231 the MX Shelf has the largest area. It acted as a strong carbon sink in winter and spring
232 (1.46 and 0.97 mol C m^{-2} yr^{-1}) and then a carbon source in summer and fall (-0.96 and -
233 0.76 mol C m^{-2} yr^{-1}). Waters along the eastern side of the MX Shelf were a sink during
234 most of the year, while to the west the shelf was a source in summer and fall. On an
235 annual scale, this region was a sink with an air-sea flux of 0.19 mol C m^{-2} yr^{-1}. To the
236 north, the WGoM Shelf has the smallest area among the four shelf sub-regions. It acted
237 as a CO_2 source during spring, summer, and fall (-0.24, -1.69 and -1.06 mol C m^{-2} yr^{-1})
238 and a strong carbon sink during winter (1.62 mol C m^{-2} yr^{-1}). On an annual scale the
239 WGoM region was a CO_2 source with a degassing rate of 0.34 mol C m^{-2} yr^{-1}.

240 The NGoM Shelf shifted from acting as a CO_2 source in summer and fall (-1.42
241 and -0.79 mol C m^{-2} yr^{-1}) to a sink in winter and spring (1.01 and 2.49 mol C m^{-2} yr^{-1}).
242 The most prominent feature here was the continuous, strong degassing in the coastal
243 waters around the Mississippi-Atchafalaya River mouths. However, as the water becomes
244 deeper, the NGoM Shelf water shifted from acting as a sink during winter and spring to a
245 source during summer and fall. Despite of the extensive degassing in the coastal water,
246 the NGoM Shelf overall was a CO_2 sink on a yearly basis (0.32 mol C m^{-2} yr^{-1}). Similarly,

247 the WF Shelf also shifted from acting as a CO_2 source in summer and fall (-1.26 and -
248 1.73 mol C m^{-2} yr^{-1}) to a sink in winter and spring (1.19 and 0.28 mol C m^{-2} yr^{-1}). The
249 degassing in the inner shelf was strong enough to make the WF Shelf a CO_2 source on a
250 yearly basis (-0.38 mol C m^{-2} yr^{-1}).

251 Despite the salient spatial and temporal variability, the GoM was an overall CO_2
252 sink, mainly because of the strong uptake in the open ocean. For validation purposes, we
253 compared (in Table 1) model-simulated air-sea flux against an estimation based on
254 observations, which utilized all available measurements collected within the GoM from
255 2005 to 2010 (Robbins et al., 2014). Our control-run estimations generally agreed with
256 in-situ measurements in all five sub-regions in terms of the ocean's role as a CO_2 source
257 or sink. There is some discrepancy in the magnitude of the estimated flux, which can be
258 attributed to 1) the spatial and temporal heterogeneity of the in-situ dataset and 2) the
259 spatially uniformed air pCO_2 used by our model.

260

261 **4.3 Model Sensitivity experiments: No-bio simulation (Exp2)**

262 To test the role of biological processes in regional pCO_2 variability, a no-bio
263 simulation was conducted, where all biology sources and sinks of DIC and alkalinity
264 were disabled similar to the experiment described in Fennel and Wilkin (2009). The
265 experiment produced higher surface pCO_2. The multi-year mean sea surface pCO_2 was
266 elevated by 88.0 ppm (from 393.1 to 466.5 ppm) for the NGoM Shelf and 56.0 ppm
267 (from 375.1 to 463.1 ppm) for the entire Gulf (Fig.6). Such pCO_2 increase was not
268 temporally uniform. On the NGoM Shelf, pCO_2 increases in the no-bio simulation was
269 clearly higher during spring-summer (84.1 and 95.6 ppm) than during fall-winter (57.3

and 56.0 ppm). On the Gulf-wide scale, the pCO_2 increase was stronger during summer (97.1 ppm) than the rest seasons (86.5, 87.6, and 80.9 ppm for spring, fall, and winter). For air-sea flux, the elevated surface pCO_2 turns all five sub-regions into a carbon source throughout the year, resulting in a net outflux rate of 2.09 mol C m^{-2} yr^{-1} (Table 1).

4.4 Model Sensitivity experiments: historical river forcing (Exp3)

Fig.4 shows that river discharge and DIC inputs during years 1904-1910 as simulated by the DLEM model were comparable with those at present (2004-2010). The multi-year mean value of freshwater discharge is 25,700 m^3/s for 1904-1910 and 23,900 m^3/s for 2004-2010. The Mississippi-Atchafalaya delivered 1.51×10^{12} mol C yr^{-1} during 1904-1910 and 1.70×10^{12} mol C yr^{-1} during 2004-2010. However, NO_3 inputs during 1904-1910 was < 30% of current inputs (18.12 vs. 63.18 $\times10^9$ mol N yr^{-1}). Limited N input led to a decrease of primary production not only on the NGoM Shelf, but also the adjacent waters on the WGoM and WF Shelves. Reduced primary production resulted in the coastal ocean being a weaker carbon sink during spring and summer (Fig. 8) and the NGoM Shelf a year-long carbon source with a net outflux rate of 0.61 mol C m^{-2} yr^{-1} (Table 1). A close examination of the spring and summer condition on the NGoM Shelf showed that differences in primary production between Exp1 and Exp3 were simulated mainly along the Texas and Louisiana coasts. Primary production was significantly elevated in the control run because of enhanced NO_3 inputs (Fig. 8a and c). Elevated primary production brought down the sea surface pCO_2. During spring, enhanced primary production and decreased CO_2 was simulated along the Louisiana and Texas coast (Fig.

292 8b), while during summer when coastal circulation was influenced by the westerly wind
293 forcing, the decreased CO_2 was more confined within waters along the Louisiana coast.
294
295 ## 5. Discussion
296 So far, the carbon dynamics in the GoM were poorly characterized and
297 represented a large uncertainty. This study provides one of the first attempts to quantify
298 GoM-wide carbon fluxes and exchanges using a coupled physical-biogeochemical model.
299 Here, we discuss the factors controlling sea surface pCO_2 variability on the river-
300 influenced NGoM Shelf and the Loop Current-influenced open ocean. The relationship
301 between pCO_2 and other hydrographic variables as well as model uncertainty are also
302 considered.
303
304 ### 5.1 NGoM Shelf
305 The Mississippi-Atchafalaya River and associated plume play the most important
306 role in determining the pCO_2 distribution on the NGoM Shelf. The large input of fluvial
307 DIC and alkalinity introduces carbonate saturation in the coastal waters, conversely,
308 nutrients from the river enhance local primary production, which results in DIC removal
309 and thus reduces sea surface pCO_2 (e.g. Lohrenz et al., 2010; Guo et al., 2012; Huang et
310 al., 2013 and 2015). Such biological removal of CO_2 was also confirmed by the elevated
311 pCO_2 values in the no-bio simulation in this study. Although the river plume's influence
312 on CO_2 flux has been addressed by prior observational studies, large uncertainties were
313 also found regarding whether the NGoM Shelf is a CO_2 sink or source over a longer time
314 period. For instance, Huang et al. (2013) found a large difference between the pCO_2

315 distributions in April 2009 and in March 2010. Such a difference was attributed to the
316 variations in river plume extension influenced by local wind conditions and river
317 discharge. In a later communication, based on ship-measurements from 11 cruises, Huang
318 et al. (2015a) concluded that the NGoM Shelf acted as a net CO_2 sink, but with a large
319 uncertainty (influx rate: 0.96 ±3.7 mol m^{-2} yr^{-1}).

320 Model results in this study revealed significant spatial and temporal gradients in
321 sea surface pCO_2 as well. The multi-year mean (2005-2010) pCO_2 distribution was
322 characterized by high values in the coastal waters (Fig. 9a), accompanied by low salinity
323 (Fig. 9c), high Dissolved Inorganic Nitrogen (DIN) and high DIC (Figs. 9d and 9e). The
324 pCO_2 value was significantly lower as water became deeper, where the ocean acted as a
325 CO_2 sink during most time of the year (Figs. 7a through d). The surface pCO_2 distribution
326 on the NGoM Shelf was highly correlated with surface salinity (r value: -0.81) and DIN
327 concentration (r value: 0.80) throughout the year, while its correlations with surface
328 temperature and DIC concentration were significant only for part of the year (for detailed
329 season-by-season correlation see Table 2). Although our model suggests that the shelf-
330 wide pCO_2 distribution was positively correlated with DIN concentration, this is not
331 contrary to findings of the above-mentioned observational studies, that is, the high DIN
332 stimulates primary production should be negatively correlated with sea surface pCO_2.
333 Instead, the high DIN concentration, together with the low salinity, was a signal of rich
334 DIC from the riverine inputs and potentially the light-limited condition within the river
335 plume. In other words, CO_2 outgassing from oversaturated plume water overwhelmed the
336 CO_2 influx induced by "biological pump" in the areas near the river mouths.

337 To further link pCO_2 dynamics with biological processes on the NGoM shelf, we
338 plotted the seasonal mean pCO_2 against surface salinity of the control and no-bio runs in
339 Fig.10. Seawater pCO_2 decreased almost linearly as salinity increased in the no-bio
340 simulation in all seasons (right panels). For most seasons of the year (except winter), the
341 NGoM shelf acted as a source of CO_2 if no biological mixing was involved. During
342 summer when discharge and river DIC input were high, the high pCO_2 low salinity
343 waters around the Mississippi River Delta (86-88°W, reddish points) can be easily
344 differentiated from the high salinity low pCO_2 waters on the Texas Shelf (92-95°W,
345 bluish points).
346 When biological processes were included, the shelf water exhibited large spatial
347 and seasonal variability (left panels). A pCO_2 minimum was simulated in mid-salinity
348 waters (30-33 psu) during spring and summer, which is consistent with the curve derived
349 by Huang et al., 2015a using ship measurements. Compared with the no-bio run, pCO_2
350 was reduced significantly and exhibited a wider range in the control run. The biological
351 removal of sea surface CO_2 was most salient in waters around the Mississippi River Delta
352 throughout a year. The difference in pCO_2 between waters around the delta and the Texas
353 Shelf became more salient. The surface pCO_2 was in general higher in the Texas Shelf
354 region than around the delta. Intriguingly, the pCO_2-salinity curve of waters around the
355 Mississippi Delta exhibited a bifurcated feature in spring and summer. We further
356 examined the relationship between salinity and variables other than pCO_2 and found a
357 similar pattern in the DIC-salinity curve (not shown here), which was also reported by
358 Guo et al., 2012 based on ship measurements. The similarity between the DIC-salinity
359 and pCO_2-salinity curves indicates that the elevated pCO_2 water in the plume and on the

Texas Shelf is a result of respiration, which is usually linked with hypoxia. We note that Hetland and DiMarco (2007) also suggested that hypoxia on the NGoM Shelf happened both in the deltaic region due to plume-dependent respiration, and on the Texas Shelf due to benthic respiration.

5.2 Open Ocean

In the open ocean, the distribution of surface pCO_2 was largely determined by that of the surface DIC (r value: 0.93) and alkalinity throughout the year (r value: -0.85, for detailed season-by-season correlations see Table 2), while the influence from DIN and primary production was limited to fall and winter months when wind-induced upwelling is strong (Xue et al., 2013). The dependence of pCO_2 on DIC and alkalinity makes the Loop Current an important factor controlling the regional air-sea CO_2 flux. In addition to a relatively high temperature, the Loop Current water is also characterized by low DIC and high alkalinity (Wang et al., 2013 and references therein). The multi-year mean sea surface temperature in Fig.9b shows persistent warm water mass in the form of the Loop Current, which carries the carbonate characteristics of the Caribbean water (i.e. low DIC and high alkalinity, Figs. 9e and 9f). Surface pCO_2 in this warm water mass was significantly lower than surrounding shelf waters (Fig. 9a), making the Loop Current a strong carbon sink throughout the year (Figs.7a-d). Any changes in the Caribbean water's carbonate characteristics will affect the carbon budget in the GoM as well as waters further downstream in the Gulf Stream.

383 **5.3 Carbon budget estimation and model uncertainty**

384 Based on our model-simulations, we conclude that the GoM is an overall CO_2
385 sink, taking up 1.11×10^{12} mol C yr^{-1} from the air. This estimation is comparable to those
386 based on in situ observations, e.g. 1.48×10^{12} mol C yr^{-1}, (Coble et al., 2010) and $0.30 \times$
387 10^{12} mol C yr^{-1} (Robbins et al. 2014). These recent estimates are in stark contrast to the
388 earlier SOCCR report (Takahashi et al. 2007), which found the GoM to be a CO_2 source
389 (1.58×10^{12} mol C yr^{-1}, the GoM and Caribbean Sea combined). In addition, we estimated
390 that the GoM received ~ 2.18×10^{12} mol C yr^{-1} from rivers, the majority of which were
391 from the Mississippi-Atchafalaya River (~1.80×10^{12} mol C yr^{-1}). These two DIC
392 sources (air: ~1.11×10^{12} mol C yr^{-1} plus river: ~2.18×10^{12} mol C yr^{-1}) largely balance
393 the DIC transported out of the GoM by the Loop Current (~ 3.30×10^{12} mol C yr^{-1}, Wang
394 et al., 2013).

395 We notice that, during summer months, our model simulated a higher surface
396 pCO_2 than ship measurements on the NGoM Shelf (Fig.6a). As discussed in Section 5.1,
397 a large part of the strong CO_2 degassing simulated by our model was from respiration on
398 the Texas Shelf. Yet a close examination of the distribution of available ship
399 measurements indicates that data points on the Texas Shelf are fairly sparse and sporadic
400 (Fig.5), which may partially explain the mismatch between model and ship measurements
401 in Fig.6a. For instance, in the summer of 2010 when more ship measurements were
402 available on the NGoM shelf, both model and observation indicated a high pCO_2 in the
403 summer. In addition, the current model resolution (~5 km) may not be high enough to
404 reproduce small-scale circulation patterns associated with the Mississippi River plume.
405 The complexity of the food web and uncertainty in model parameterization (e.g.

406 rudimentarily represented particular organic matters, the lack of phosphate and silicate
407 components, etc.) warrants further investigation.
408

409 ## 6. Summary

410 A coupled physical-biogeochemical model was used to hindcast surface pCO_2 in
411 the GoM from January 2004 to December 2010. Favorable comparisons were found
412 when validating model solutions against ship measurements on the Gulf-wide scale,
413 indicating that this coupled model can reproduce observed pCO_2 variability in the GoM.
414 Time series of spatially averaged pCO_2 for both shelf and open ocean waters exhibit
415 significant seasonal variability, with high values in August and low values in February.
416 Model-simulated pCO_2 values were elevated by 56 and 88 ppm for the entire Gulf and
417 the NGoM shelf, respectively, when the biological sources and sinks of carbon were
418 disabled (i.e., the no-bio simulation). Without biological processes, the GoM shifts to a
419 strong carbon source with a outflux rate of 2.10 mol C m^{-2} yr^{-1}. Another sensitivity test
420 driven by river conditions from the 1904-1910 period (reduced NO_3 and comparable DIC)
421 indicates the NGoM shelf could have been a CO_2 source with an outflux rate of 0.61 mol
422 C m^{-2} yr^{-1} under those conditions.

423 The Mississippi-Atchafalaya River plume is the dominant factor controlling the
424 pCO_2 distribution on the NGoM Shelf. Although the NGoM Shelf is overall a CO_2 sink,
425 high surface pCO_2 was simulated in relative shallow waters, induced by both
426 oversaturated plume water and respiration on different parts of the shelf. pCO_2 in the
427 open ocean is controlled largely by the low DIC high alkalinity Loop Current water from
428 the Caribbean Sea.

Our model simulations characterize the GoM as an overall CO_2 sink, taking up ~ 1.11×10^{12} mol C yr^{-1} from the air. Together with the enormous riverine input (~ 2.18×10^{12} mol C yr^{-1}), this carbon influx was largely balanced by carbon export through the Loop Current estimated by an earlier study. More accurate model predictions of water column DIC concentration will require more in-situ data for improved specification of model DIC initial conditions, and further refinements in model parameterizations to better account for complex carbon dynamics in the coastal ocean.

Acknowledgement

Research support provided through the National Aeronautics and Space Administration (NNX10AU06G, NNX12AP84G, NNX14AO73G, and NNH13ZDA001N); National Science Foundation (OCE-0752254 and OCE-0752110); NOAA Grant NA11NOS0120033; and GRI GISR grant SA/GoMRI-006 and GOMRI-020 is much appreciated. The operational mode of the SABGOM model is located at http://omgsrv1.meas.ncsu.edu:8080/ocean-circulation/. Data of daily nowcast/forecast model output is hosted at http://omgsrv1.meas.ncsu.edu:8080/thredds/sabgom_catalog.html. Data used in all figures for the hindcast simulation can be obtained by contacting the corresponding author.

References

AIRS (2008), AIRS/Aqua Level 3 Monthly CO_2 in the free troposphere (AIRS+AMSU),version 005, edited by G. E. S. D. a. I. S. C. G. DISC), Greenbelt, MD, USA.

Aulenbach, B. T., H. T. Buxton, W. T. Battaglin, and R. H. Coupe (2007), Streamflow and nutrient fluxes of the Mississippi-Atchafalaya River Basin and subbasins for the period of record through 2005: U.S. Geological Survey Open-File Report 2007-1080 Rep.

Bauer, J. E., W.-J. Cai, P. A. Raymond, T. S. Bianchi, C. S. Hopkinson, and P. A. G. Regnier (2013), The changing carbon cycle of the coastal ocean, Nature, 504(7478), 61-70.

Benway, H. M., and P. G. Coble (2014), Introduction. Report of The U.S. Gulf of Mexico Carbon Cycle Synthesis Workshop, Ocean Carbon and Biogeochemistry Program and North American Carbon Program Rep., 63 pp.

Cai, W.-J. (2003), Riverine inorganic carbon flux and rate of biological uptake in the Mississippi River plume, Geophys. Res. Lett., 30(2), 1032.

Cai, W.-J. (2011a), Estuarine and Coastal Ocean Carbon Paradox: CO_2 Sinks or Sites of Terrestrial Carbon Incineration?, Annual Review of Marine Science, 3(1), 123-145.

Cai, W.-J., et al. (2011b), Acidification of subsurface coastal waters enhanced by eutrophication, Nature Geosci, 4(11), 766-770.

Chassignet, E. P., H. E. Hurlburt, O. M. Smedstad, G. R. Halliwell, P. J. Hogan, A. J. Wallcraft, R. Baraille, and R. Bleck (2007), The HYCOM (HYbrid Coordinate Ocean Model) data assimilative system, Journal of Marine Systems, 65(1-4), 60-83.

Chavez, F. P., T. Takahashi, W. J. Cai, G. Friederich, B. Hales, R. Wanninkhof, and R. A. Feely (2007), Coastal OceansRep., National Climatic Data Center, Asheville, NC, USA.

Coble, P. G., L. L. Robbins, K. L. Daly, W. J. Cai, K. Fennel, and S. E. Lohrenz (2010), A preliminary carbon budget for the Gulf of Mexico, Ocean Carbon and Biogeochemistry News, 3(3), 1-4.

Feely, R. A., C. L. Sabine, K. Lee, W. Berelson, J. Kleypas, V. J. Fabry, and F. J. Millero (2004), Impact of Anthropogenic CO_2 on the $CaCO_3$ System in the Oceans, Science, 305(5682), 362-366.

Fennel, K. (2010), The role of continental shelves in nitrogen and carbon cycling: Northwestern North Atlantic case study, Ocean Sci, 6(2), 539-548.

Fennel, K., R. Hetland, Y. Feng, and S. DiMarco (2011), A coupled physical-biological model of the Northern Gulf of Mexico shelf: model description, validation and analysis of phytoplankton variablity, Biogeosciences, 8, 1881-1899.

Fennel, K., and J. Wilkin (2009), Quantifying biological carbon export for the northwest North Atlantic continental shelves, Geophys Res Lett, 36(18), L18605.

Fennel, K., J. Wilkin, J. Levin, J. Moisan, J. O'Reilly, and D. B. Haidvogel (2006), Nitrogen cycling in the Middle Atlantic Bight: results from a three-dimensional model and implications for the North Atlantic nitrogen budget, Global Biogeochemical Cycles, 20, GB3007, doi: 10.1029/2005GB002456.

493 Fennel, K., J. Wilkin, M. Previdi, and R. Najjar (2008), Denitrification effects on air-sea
494 CO_2 flux in the coastal ocean: simulations for the Northwest North Atlantic,
495 Geophysical Research Letter, 35(L24608), doi: 10.1029/2008GL036147.
496 Fuentes-Yaco, C., D. A. S. de Leon, M. A. Monreal-Gomez, and F. Vera-Herrera (2001),
497 Environmental forcing in a tropical estuarine ecosystem: the Palizada River in the
498 southern Gulf of Mexico, Mar Freshwater Res, 52(5), 735-744.
499 Gledhill, D. K., R. Wanninkhof, F. J. Millero, and M. Eakin (2008), Ocean acidification
500 of the Greater Caribbean Region 1996-2006.
501 Guo, X., et al. (2012), Carbon dynamics and community production in the Mississippi
502 River plume, Journal Limnology and Oceanography, 57(1), 1-17.
503 Haidvogel, D. B., et al. (2008), Ocean forecasting in terrain-following coordinates:
504 Formulation and skill assessment of the Regional Ocean Modeling System, Journal of
505 Computational Physics, 227(7), 3595-3624.
506 He, R., K. Chen, K. Fennel, G. Gawarkiewicz, and D. McGillicuddy (2011), Seasonal
507 and interannual variability of physical and biological dynamics at the shelfbreak
508 front of the Middle Atlantic Bight: Nutrient supply mechanisms. Biogeosciences, 8,
509 2935-2946, doi: 10.5194/bgd-8-1555-2011
510 Hetland, R., and S. DiMarco (2007), How does the character of oxygen demand control
511 the structure of hypoxia on the Texas-Louisiana continental shelf?, Journal of Marine
512 Systems, 70, 49-62.
513 Hofmann, E. E., B. Cahill, K. Fennel, M. A. Friedrichs, K. Hyde, C. Lee, A. Mannino, R.
514 G. Najjar, J. E. O'Reilly, and J. Wilkin (2011), Modeling the dynamics of continental
515 shelf carbon, Annual review of marine science, 3, 93-122.

516 Huang, W.-J., W. J. Cai, R. Castelao, W. Y, and S. E. Lohrenz (2013), Effects of a wind-
517 driven cross-shelf large river plume on biological production and CO2 uptake on the
518 Gulf of Mexico during spring, Limnology and Oceanography, 58(5), 1727-1735.
519 Huang, W. J., W. J. Cai, Y. Wang, S. E. Lohrenz, and M. C. Murrell (2015a), The carbon
520 dioxide system on the Mississippi River‐dominated continental shelf in the northern
521 Gulf of Mexico: 1. Distribution and air‐sea CO_2 flux, Journal of Geophysical
522 Research: Oceans, 120(3), 1429-1445.
523 Huang, W. J., Cai, W. J., Wang, Y., Hu, X., Chen, B., Lohrenz, S.E., Chakraborty, S., He,
524 R., Brandes, J., Hopkinson, C.S., (2015b). The response of inorganic carbon
525 distributions and dynamics to upwelling-favorable winds on the northern Gulf of
526 Mexico during summer. Cont. Shelf Res. doi:10.1016/j.csr.2015.08.020
527 Jiang, L. Q., W. J. Cai, R. Wanninkhof, Y. C. Wang, and H. Luger (2008), Air-sea CO_2
528 fluxes on the US South Atlantic Bight: Spatial and seasonal variability, J Geophys
529 Res-Oceans, 113(C7), doi: 10.1029/2007JC004366.
530 Lee, K., L. T. Tong, F. J. Millero, C. L. Sabine, A. G. Dickson, C. Goyet, G. H. Park, R.
531 Wanninkhof, R. A. Feely, and R. M. Key (2006), Global relationships of total
532 alkalinity with salinity and temperature in surface waters of the world's oceans,
533 Geophys Res Lett, 33(19), doi: 10.1029/2006GL027207
534 Lee, K., R. Wanninkhof, R. A. Feely, F. J. Millero, and T.-H. Peng (2000), Global
535 relationships of total inorganic carbon with temperature and nitrate in surface
536 seawater, Global Biogeochemical Cycles, 14(3), 979-994.

537 Lohrenz, S. E., W. J. Cai, F. Z. Chen, X. G. Chen, and M. Tuel (2010), Seasonal
538 variability in air-sea fluxes of CO2 in a river-influenced coastal margin, J Geophys
539 Res-Oceans, 115, doi: 10.1029/2009JC005608.
540 Mehrbach, C., C. H. Culberson, J. E. Hawley, and R. M. Pytkowicx (1973),
541 MEASUREMENT OF THE APPARENT DISSOCIATION CONSTANTS OF
542 CARBONIC ACID IN SEAWATER AT ATMOSPHERIC PRESSURE1, Limnology
543 and Oceanography, 18(6), 897-907.
544 Millero, F. J. (1995), Thermodynamics of the carbon dioxide system in the oceans,
545 Geochimica et Cosmochimica Acta, 59(4), 661-677.
546 Milliman, J. D., and K. L. Farnsworth (2011), River discharge to the coastal ocean : a
547 global synthesis, 384 pp., Cambridge University Press, Cambridge ; New York.
548 Murrell, M. C., R. S. Stanley, and J. C. Lehrter (2013), Plankton community respiration,
549 net ecosystem metabolism, and oxygen dynamics on the Louisiana continental shelf:
550 implications for hypoxia, Continental Shelf Research, 52, 27-38.
551 Nixon, S. W., et al. (1996), The fate of nitrogen and phosphorus at the land sea margin of
552 the North Atlantic Ocean, Biogeochemistry, 35(1), 141-180.
553 Orr, J. C., et al. (2005), Anthropogenic ocean acidification over the twenty-first century
554 and its impact on calcifying organisms, Nature, 437(7059), 681-686.
555 Orr, J. C., R. Najjar, C. L. Sabine, and F. Joos (1999), OCMIP Abiotic-HOWTO,
556 http://www.ipsl.jussieu.fr/OCMIP/phase2/simulations/Abiotic/HOWTO-Abiotic.html,
557 edited.

558 Rabalais, N., R. E. Turner, and W. J. J. Wiseman (2002), GULF OF MEXICO
559 HYPOXIA, A.K.A. THE DEAD ZONE, Annual Review of Ecology and Systematics,
560 33, 235-263.
561 Robbins, L. L., R. Wanninkhof, L. Barbero, X. Hu, S. Mitra, S. Yvon-Lewis, W. Cai, W.
562 Huang, and T. Ryerson (2014), Air-Sea Exchange.Report of The U.S. Gulf of Mexico
563 Carbon Cycle Synthesis Workshop, Ocean Carbon and Biogeochemistry Program and
564 North American Carbon ProgramRep., 63 pp.
565 Sabine, C. L., et al. (2004), The oceanic sink for anthropogenic CO_2, Science, 305(5682),
566 367-371.
567 Sabine, C. L., and T. Tanhua (2010), Estimation of anthropogenic CO_2 inventories in the
568 ocean, Annual Review of Marine Science, 2(1), 175-198.
569 Shchepetkin, A. F., and J. C. McWilliams (2005), The regional ocean modeling system
570 (ROMS): a split-explicit, free-surface, topography-following coordinates ocean
571 model, Ocean Modelling, 9, 347-404.
572 Signorini, S. R., A. Mannino, R. G. Najjar, M. A. M. Friedrichs, W.-J. Cai, J. Salisbury,
573 Z. A. Wang, H. Thomas, and E. Shadwick (2013), Surface ocean pCO_2 seasonality
574 and sea-air CO_2 flux estimates for the North American east coast, Journal of
575 Geophysical Research: Oceans, 118(10), 5439-5460, doi: 10.1002/jgrc.20369.
576 Stocker, T., D. Qin, G.-K. Plattner, M. Tignor, S. K. Allen, J. Boschung, A. Nauels, Y.
577 Xia, V. Bex, and P. M. Midgley (2014), Climate change 2013: The physical science
578 basis, Cambridge University Press Cambridge, UK, and New York.

579 Sturges, W., and R. Leben (2000), Frequency of Ring Separations from the Loop Current
580 in the Gulf of Mexico: A Revised Estimate, Journal of Physical Oceanography, 30(7),
581 1814-1819.
582 Takahashi, T., S. C. Sutherland, and A. Kozyr (2015), Global Ocean Surface Water
583 Partial Pressure of CO_2 Database: Measurements Performed During 1957-2012
584 (Version 2014), Carbon Dioxide Information Analysis Center, Oak Ridge National
585 Laboratory, U.S. Department of Energy, Oak Ridge, Tennessee.
586 Tian, H., et al. (2015), Climate extremes dominate seasonal and interannual variations in
587 carbon export from the Mississippi River Basin, Global Biogeochemical Cycles, 29.
588 29-37.
589 Toner, M., A. D. Kirwan, A. C. Poje, L. H. Kantha, F. E. Muller-Karger, and C. K. R. T.
590 Jones (2003), Chlorophyll dispersal by eddy-eddy interactions in the Gulf of Mexico,
591 J Geophys Res-Oceans, 108(C4), doi: 10.1029/2002JC001499.
592 Tsunogai, S., S. Watanabe, and T. Sato (1999), Is there a "continental shelf pump" for the
593 absorption of atmospheric CO_2?, Tellus B, 51(3), 701-712.
594 Uppström, L. R. (1974), The boron/chlorinity ratio of deep-sea water from the Pacific
595 Ocean, paper presented at Deep Sea Research and Oceanographic Abstracts, Elsevier.
596 Wang, Z. A., R. Wanninkhof, W.-J. Cai, R. H. Byrne, X. Hu, T.-H. Peng, and W.-J.
597 Huang (2013), The marine inorganic carbon system along the Gulf of Mexico and
598 Atlantic coasts of the United States: Insights from a transregional coastal carbon
599 study, Limnology and Oceanography, 58(1), 325-342.
600 Wanninkhof, R. (1992), Relationship between wind-speed and gas-exchange over the
601 Ocean, J Geophys Res-Oceans, 97(C5), 7373-7382, doi: 10.1029/92JC00188.

602 Weiss, R. F. (1974), Carbon dioxide in water and seawater: the solubility of a non-ideal
603 gas, Marine Chemistry, 2(3), 203-215.
604 Weiss, R. F., and B. A. Price (1980), Nitrous oxide solubility in water and seawater,
605 Marine Chemistry, 8(4), 347-359.
606 Xue, Z., R. He, K. Fennel, W. Cai, S. Lohrenz, and C. Hopkinson (2013), Modeling
607 Seasonal and Interannual Variability of Circulation and Biogeochemical Processes in
608 the Gulf of Mexico, Biogeosciences, 10, 7219-7234.
609 Xue, Z., J. Zambon, Z. Yao, Y. Liu, and R. He (2015), An Integrated Ocean Circulation,
610 Wave, Atmosphere and Marine Ecosystem Prediction System for the South Atlantic
611 Bight and Gulf of Mexico, Journal of Operational Oceanography, 8(1)
612 Zeebe, R., and D. Wolf-Gladrow (2001), CO_2 in Seawater: Equilibrium, Kinetics,
613 Isotopes, Elsevier, Amsterdam.
614

615 ## Tables and Figures

616 Table 1. Comparison between observed and modeled air-sea CO_2 flux. Observations are
617 taken from Robins et al (2014), whereas the model results are seven-year (2005-2010)
618 model mean*.

		Sub-regions					Gulf-wide**
		Mexico Shelf	**Texas Shelf**	**Louisiana Shelf**	**West Florida Shelf**	**Open Ocean**	
Subregion Area (10^{12} m^2)		0.18	0.08	0.15	0.15	1.01	1.56
Simulation 1 (control run)*	Spring	0.97	-0.24	1.01	0.28	1.51	1.23
	Summer	-0.96	-1.69	-1.42	-1.26	-0.33	-0.62
	Fall	-0.76	-1.06	-0.79	-1.73	0.56	0.06
	Winter	1.49	1.62	2.49	1.19	2.44	2.21
	Annual	**0.19**	**-0.34**	**0.32**	**-0.38**	**1.04**	**0.71**
Robbins et al., 2014	**Annual**	**0.09**	**-0.18**	**0.44**	**-0.37**	**0.48**	**0.19**
Simulation 2 (no-bio)	Annual	-2.77	-2.02	-1.64	-1.79	-2.08	-2.10
Simulation 3 1904-1910	Annual	0.08	-0.77	-0.61	-0.55	0.86	0.50

619

620 *unit: mol m^{-2} yr^{-1}, + indicates ocean is an air CO_2 sink; - indicates a CO_2 source to the
621 atmosphere

622 **Gulf-wide value is a sum of all sub-regions.

623

Table 2. Spatial correlation coefficients between pCO_2, sea surface temperature (SST), sea surface salinity (SSS), dissolved inorganic nitrate (DIN: NO_3+NH_4), dissolved inorganic carbon (DIC), alkalinity(ALK), and primary production (P-Prod) on the Louisiana Shelf and in the open ocean (multi-year mean of 2005-2010, control run).

Correlation Coefficient (R value)		**SST**	**SSS**	**DIC**	**DIN**	**ALK**	**P-Prod**
pCO_2 on the Louisiana Shelf	Spring	-0.24	**-0.81**	-0.12	**0.86**	-0.77	0.36
	Summer	0.63	**-0.65**	0.65	**0.66**	-0.17	0.35
	Fall	-0.66	**-0.87**	0.86	**0.78**	0.17	0.58
	Winter	-0.67	**-0.89**	0.45	**0.89**	-0.90	0.23
	Annual	-0.64	**-0.82**	0.63	**0.82**	-0.65	0.47
pCO_2 in open ocean	Spring	0.11	0.17	**0.76**	-0.27	**-0.70**	-0.41
	Summer	-0.11	-0.11	**0.99**	-0.29	**-0.91**	-0.43
	Fall	0.04	0.08	**0.96**	-0.77	**-0.88**	-0.76
	Winter	0.04	-0.05	**0.75**	-0.49	**-0.69**	-0.55
	Annual	-0.17	0.05	**0.93**	-0.50	**-0.85**	-0.59

631 Figure 1. Domain of the South Atlantic Bight and Gulf of Mexico (SABGOM) ROMS
632 model with water depth in color (unit: m). Also shown are the five sub-regions used in
633 this study, which are Mexico Shelf (MX), Western Gulf of Mexico Shelf (WGoM),
634 Northern Gulf of Mexico Shelf (NGoM), West Florida Shelf (WF), and open ocean.
635

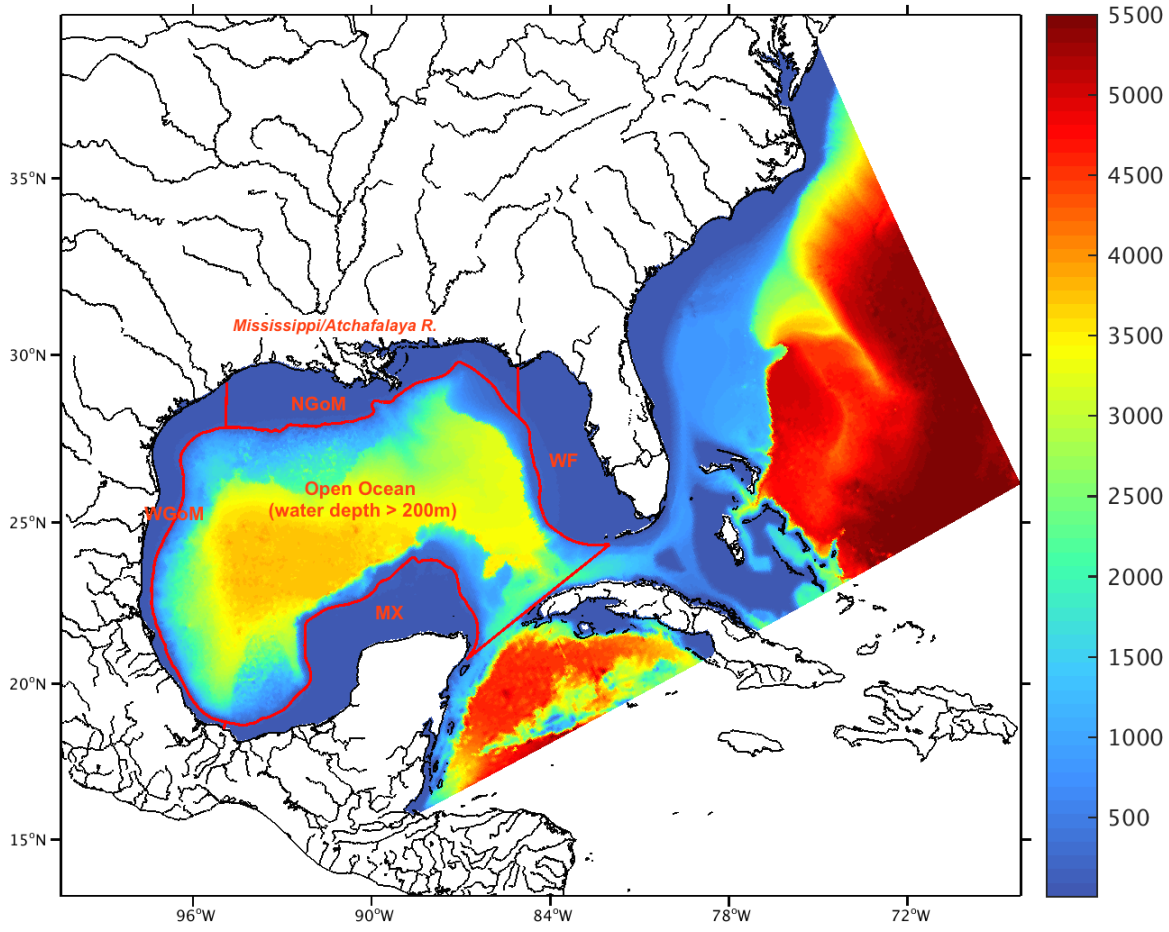

636

637 Figure 2. DIC and alkalinity initial conditions derived from the empirical relationship by

638 Lee et al., (2000 and 2006).

639

640

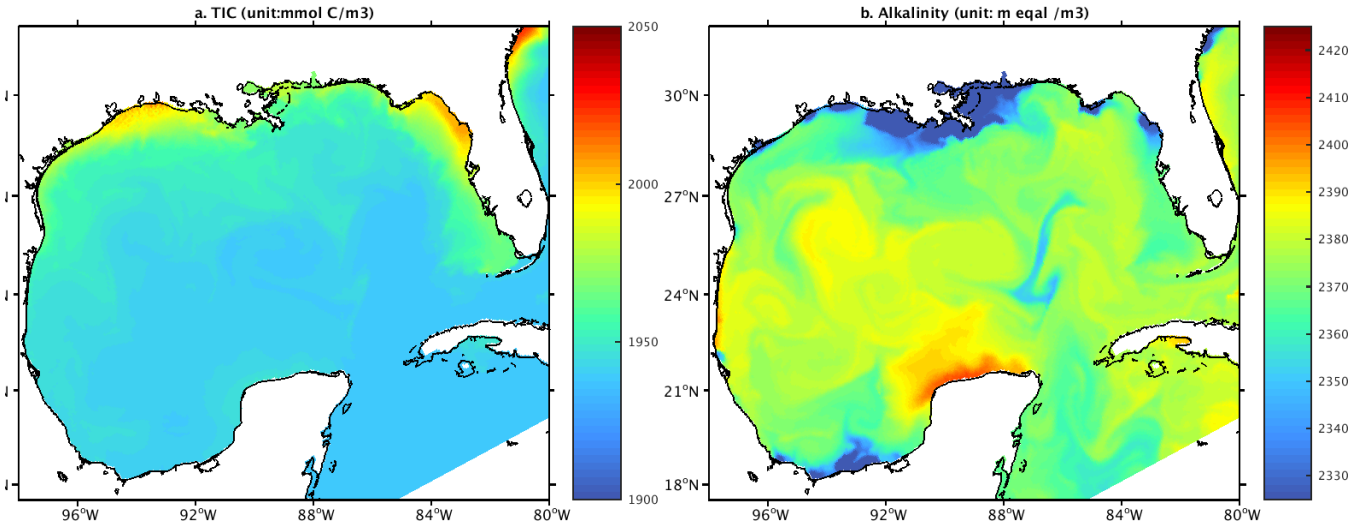

641 Figure 3. Satellite observed monthly pCO_2 (AIRS) averaged over the Gulf of Mexico (red
642 stars) and the pCO_2 air used in model air-sea CO_2 flux calculation (blue line), which is
643 generated using the curve-fitting software CCGCRV.

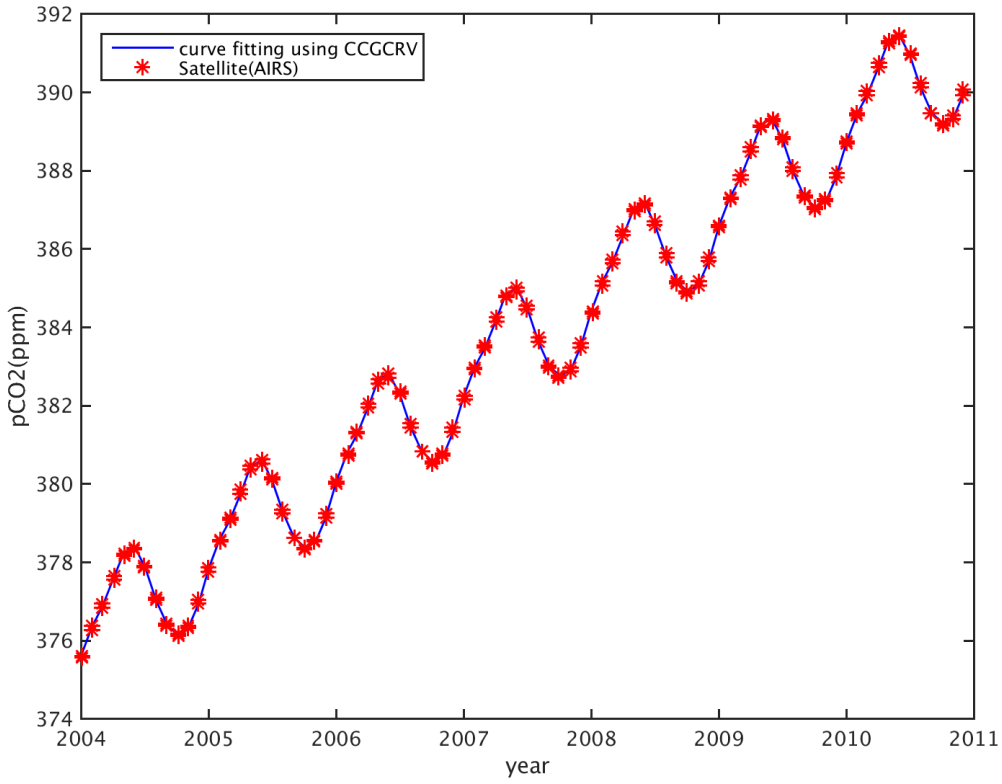

644

645 Figure 4. Comparisons between the 2005-2010 riverine DIC and NO_3 conditions
646 observed by USGS (red line) and the 1904-1910 river condition simulated by the
647 Dynamic Land Ecosystem Model (black line, Tian et al., 2015).
648

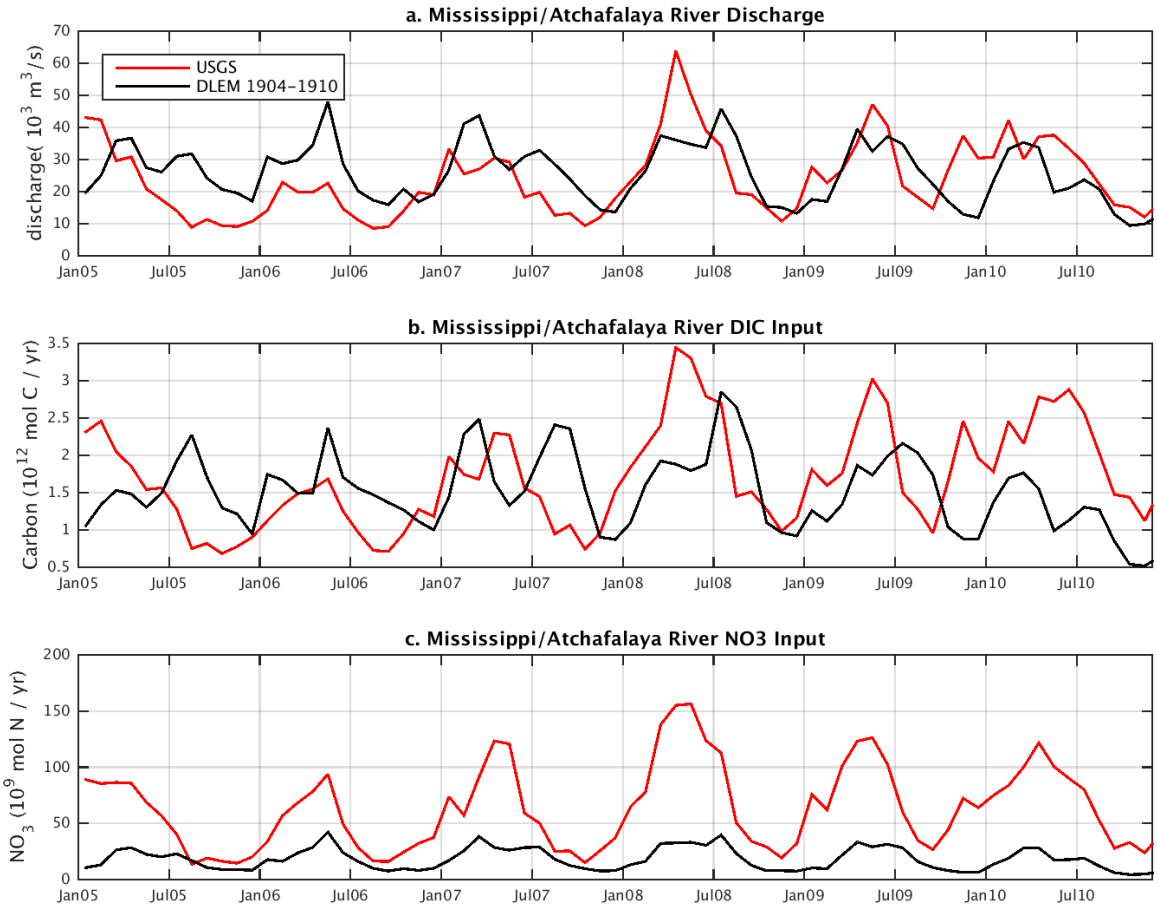

649

650 Figure 5. Locations of in-situ measurements from the LDEO database (blue) and Huang

651 et al. (2015, grey) in the period of 2005-2010.

652

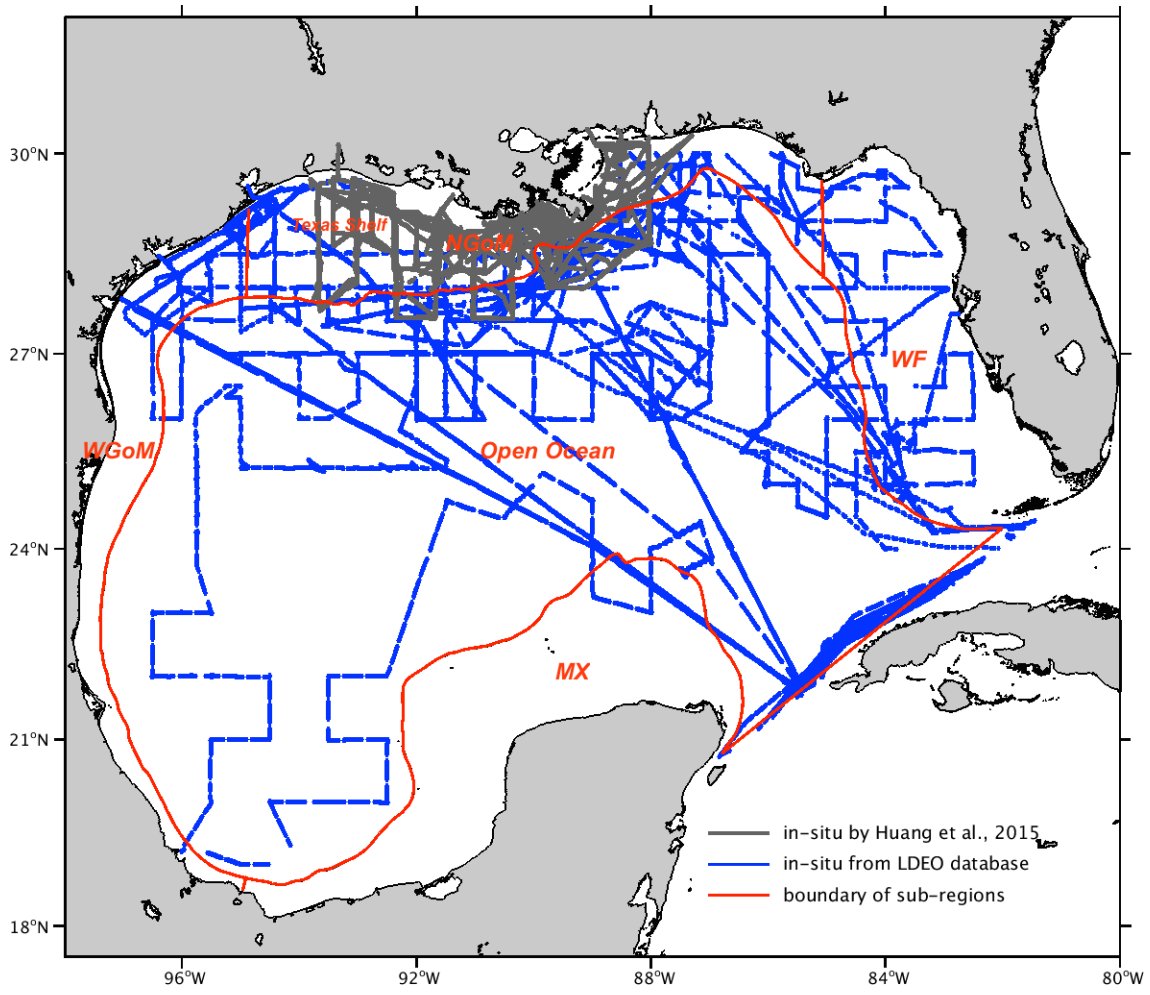

653

654 Figure 6. Time series of spatially averaged pCO_2 (control run in blue and no-bio
655 simulation in red) (a) on the Louisiana shelf, and (b) in the entire Gulf of Mexico,
656 overlaid with in situ observations (in black) from Huang et al. (2015a and b), and
657 Takahashi et al. (2015).
658

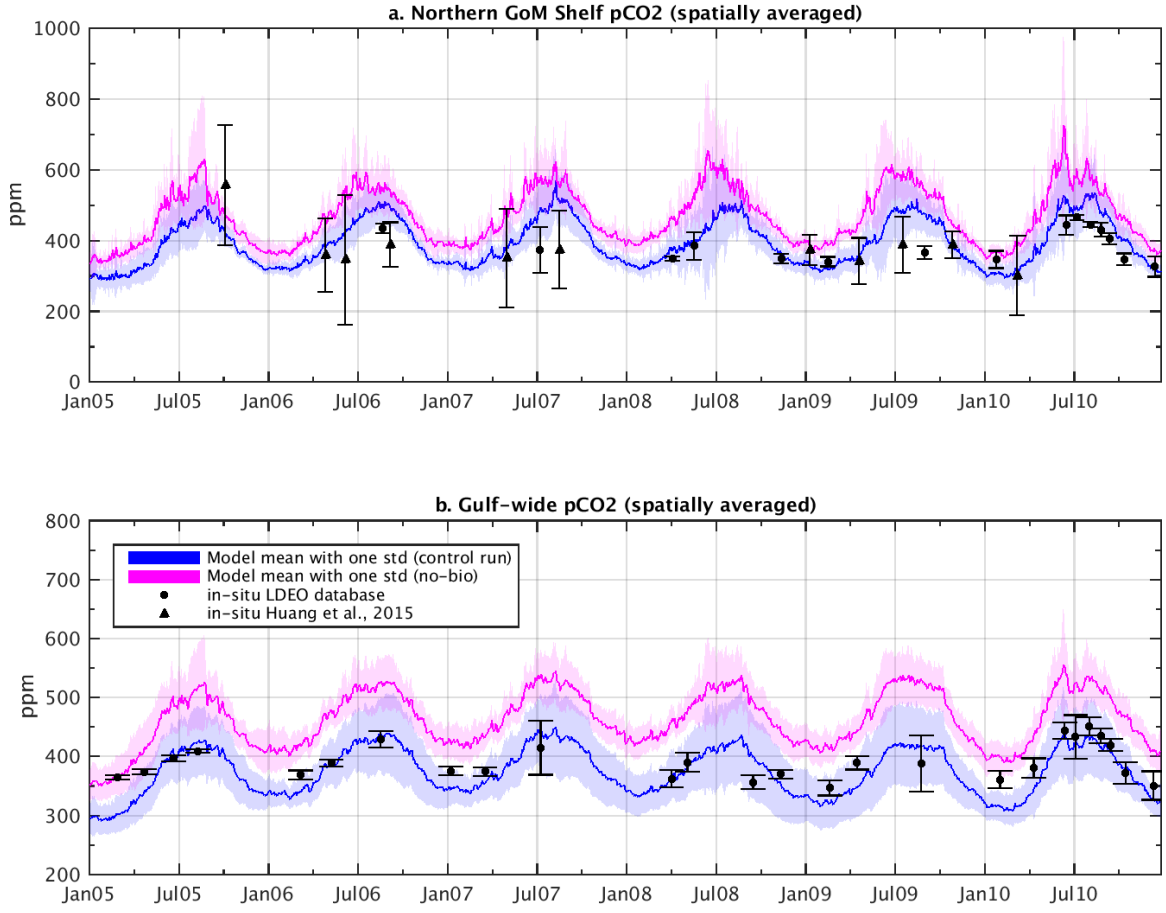

659

Figure 7. Seven-year (2005-2010) model (control run) mean air-sea CO_2 flux in the Gulf of Mexico during (a) spring, (b) summer, (c) autumn, and (d) winter. Blue color indicates where the ocean is a sink for CO_2; red color indicates where the ocean is a source.

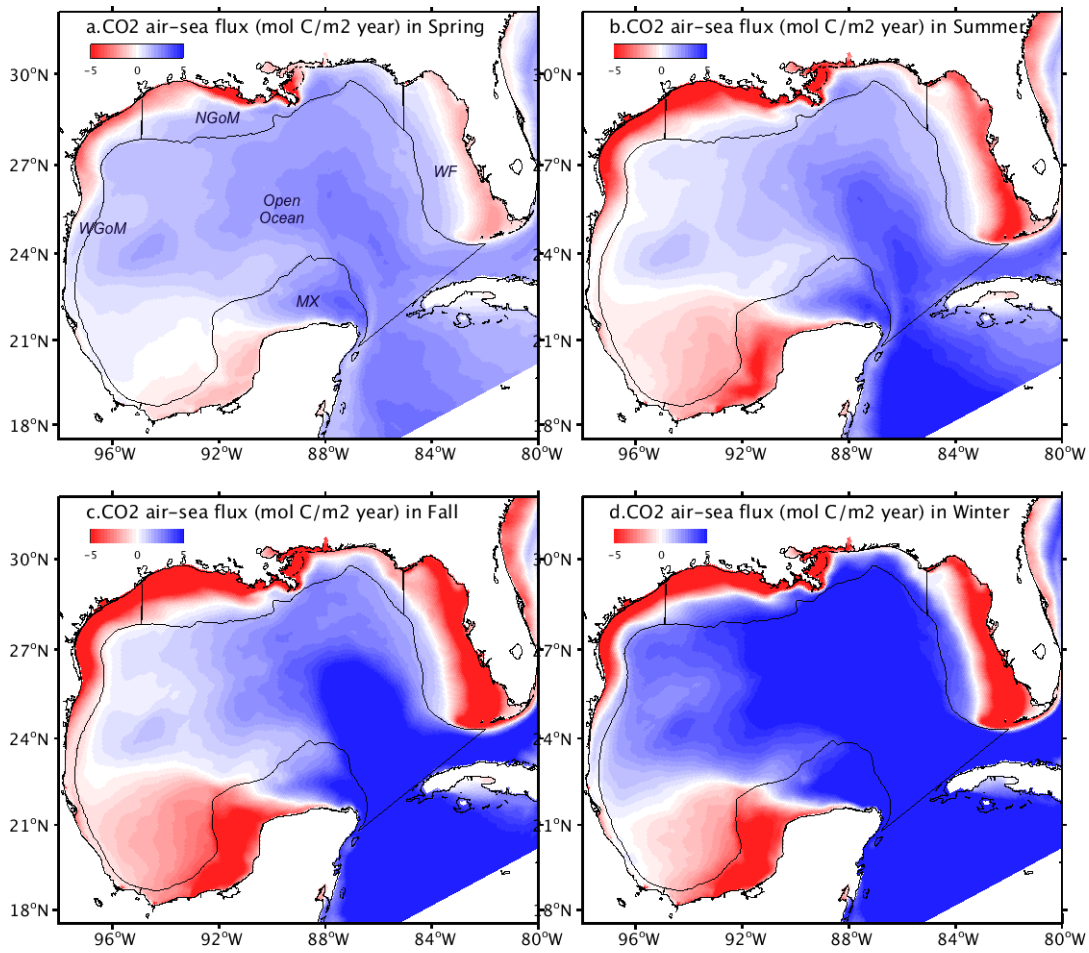

665 Figure 8. Differences in model simulated primary production and pCO_2 between the
666 2004-2010 and the 1904-1910 periods (2005-2010 minus 1905-1910 seasonal mean
667 condition). For a) and c) blue color indicates increased primary production during 2004-
668 2010, for b) and d) red color indicates reduced pCO_2 during 2004-2010.
669

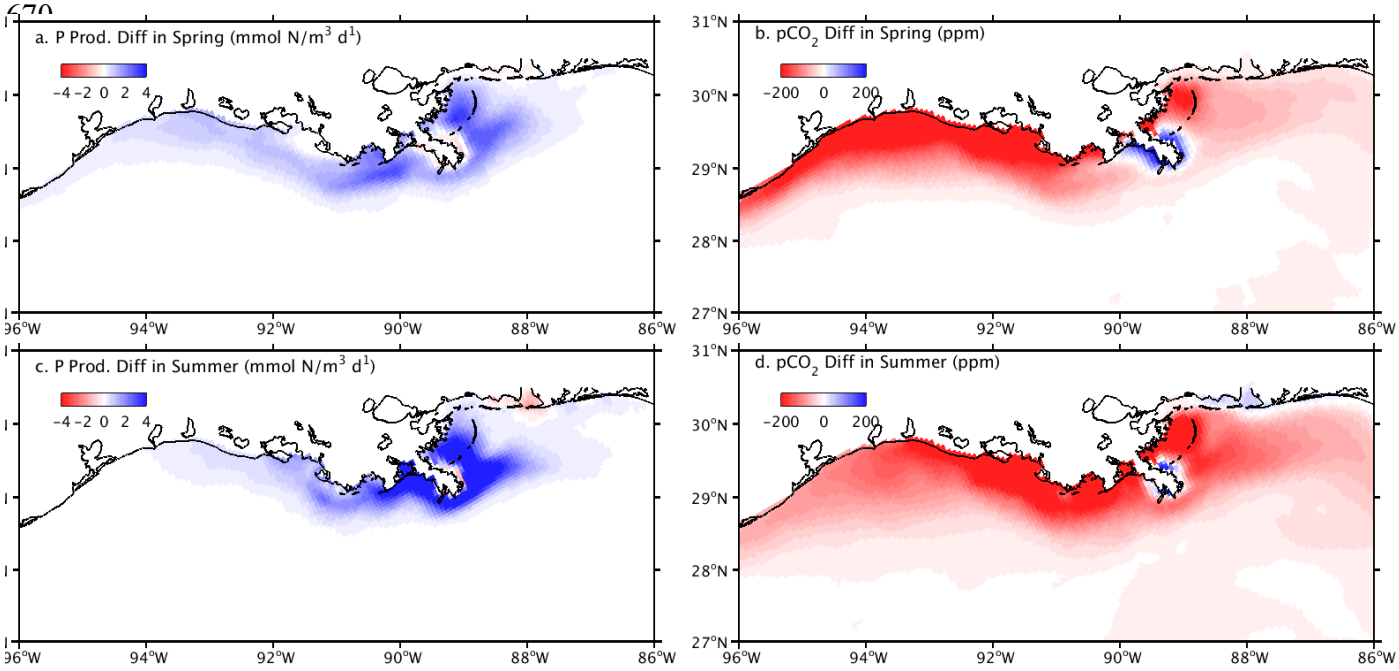

671 Figure 9. Seven-year mean (2005-2010) surface conditions simulated by the model for a)
672 pCO_2 (ppm), b) temperature (degree C), c) salinity (psu), d) dissolved inorganic carbon
673 (mmol C m^{-3}), e) dissolved inorganic nitrogen (NO_3+NH_4) (mmol N m^{-3}), and f)
674 alkalinity (mEq m^{-3}).
675

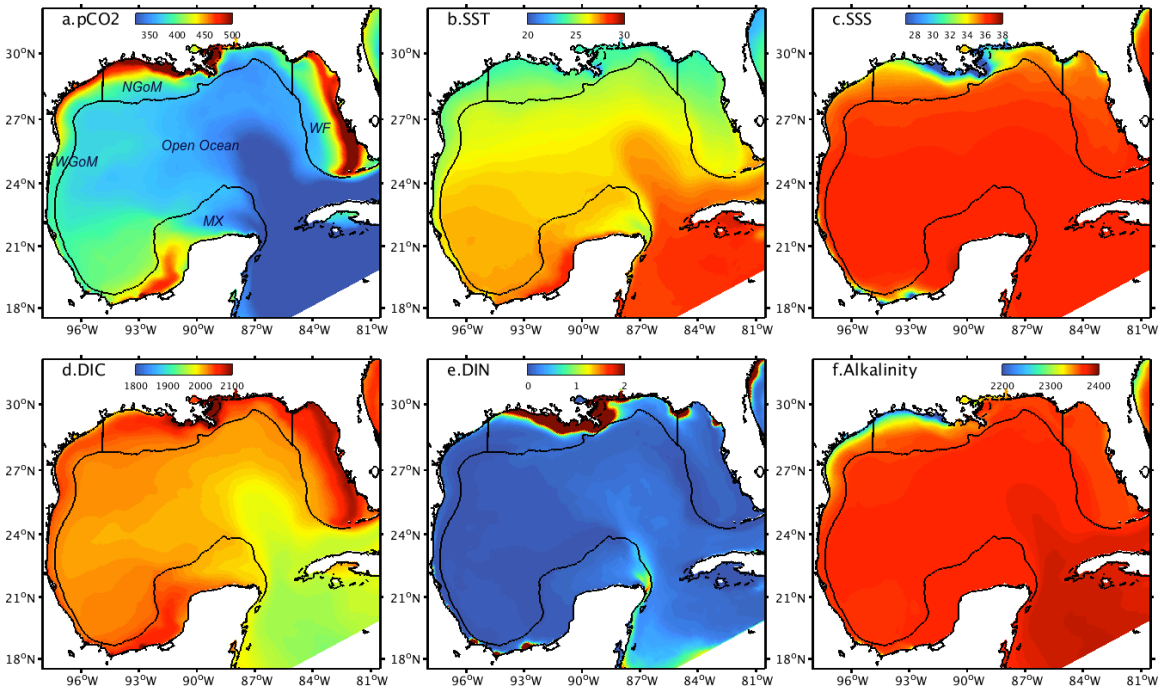

676
677
678
679

Figure 10. Seasonal mean (2005-2010) of model simulated sea surface pCO_2 against salinity for the control (a, c, e and g) and no-bio experiment (b, d, f and h) on the Louisiana Shelf; also shown are longitude with colors, note the Mississippi river delta is located around 89°W.

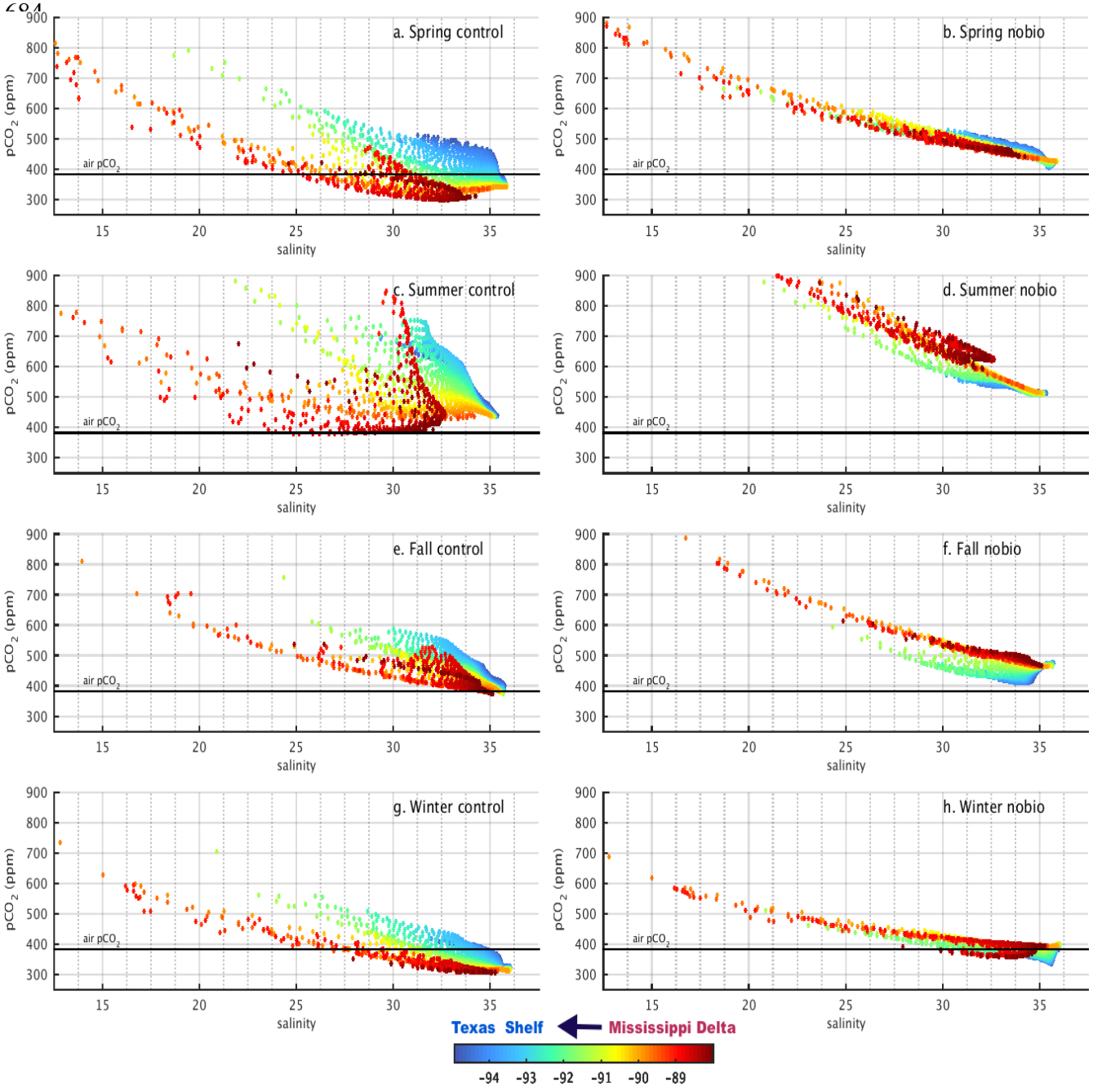

Supplementary Materials

S1. Calculation of seawater pCO_2

The seawater pCO_2 was calculated following Zeebe and Wolf-Gladrow (2001) as following:

$$pCO_2=DIC*[H^+]^2/([H^+]^2+K_1*[H^+]+K_1*K_2)/f \quad (1)$$

where DIC is the dissolved inorganic carbon and was given by model input. K_1 and K_2 are constant of carbonic acid, $K_1=[H^+]*[HCO_3^-]/[H_2CO_3]$, $K_2=[H^+]*[CO_3^{2-}]/[HCO_3]$ and were calculated following Millero (1995) using data from Mehrbach et al. (1973) as following:

$$logK_1=62.008-1/T*3670.7-logT*9.7944+S*(0.0118-S*0.000116) \quad (2)$$

$$logK_2=-4.777-1/T*1394.7-logT*9.7944+S*(0.0184-S*0.000118) \quad (3)$$

where in (2) and (3) the T is for water temperature (unit: K) and S is for salinity (unit: psu);

The f in (1) is the correction term for non-ideality and was calculated from Weiss and Price (1980) using equation 13 with 6 values. $[H^+]$ is solved using the 5th order polynomial bracket and bisection method with the following 5 coefficients:

$$p5=1; \quad (4)$$

$$p4=-Alk-K_b-K_1; \quad (5)$$

$$p3=DIC*K_1-Alk*(K_b+K_1)+K_b*borate+K_w-K_b*K_1-K_1*K_2; \quad (6)$$

$$p2=DIC*(K_b*K_1+2*K_1*K_2)-Alk*(K_b*K_1+K_1*K_2)+ K_b*borate*K_1+(K_w*K_b+K_w*K_1-K_b*K_1*K_2); \quad (7)$$

$$p1=2*DIC*K_b*K_1*K_2-Alk*K_b*K_1*K_2+K_b*borate*K_1*K_2+ K_w*K_b*K_1+K_w*K_1*K_2; \quad (8)$$

$$p0=K_w*K_b*K_1*K_2; \quad (9)$$

where *Alk* is for total alkalinity (unit: milli-equivalent per liter) and was given by model input; K_w is ion product of water ($[H^+]*[OH^-]$) and K_b is the constant of boric acid ($[H^+]*[BO_2^-]/[HBO_2]$), which were calculated following Millero (1995):

$$lnK_b=-8966.90+2890.51*S^{0.5}-77.942*S+1.726*S^{1.5}-0.0993*S^2)/T +(148.0248+137.194*S^{0.5}+1.62247*S +(-24.4344-25.085*S^{0.5}-0.2474*S)*lnT+0.053105*S^{0.5}*T) \quad (10)$$

$$lnK_w=148.9802-13847.26/T-23.6521*lnT +(-0.977+118.67/T+1.0495*lnT)*S^{0.5}-0.01615*S) \quad (11)$$

and borate stands for the concentrations for borate and was calculated following Uppstrom (1974):

$$borate=0.000232*S/1.80655/10.811 \quad (12)$$

S2. Air-Sea CO_2 flux calculation

The air-sea CO2 flux was calculated following Wanninkhof (1992) as following:

$$F=K*(pCO_{2\ air}- pCO_{2\ water}) \quad (13)$$

where pCO_2 air is the air pCO_2, and $pCO_{2\ water}$ was calculated from (1); F is the air-sea CO_2 flux (unit: millimole C meter^{-2} day^{-1});

$$K=kL \quad (14)$$

where L is the solubility of CO_2 and was calculated following Weiss (1974) as following:

$$ln\ L= -60.2409+93.4517/T+23.3585*Log(T) +S*(0.023517+T*(-0.023656+0.0047036*T)) \quad (15)$$

and the k in (14) is the gas transfer velocity and was calculated using

$$k=0.31u^2(Sc/660)^{-0.5} \quad (16)$$

where u is the wind speed at 10 m above sea-level from the North America Regional Reanalysis dataset; Sc is the Schmidt number and was set to

$$Sc=2073.1-125.62*T+36276*T^2-0.043219*T^3 \quad (17)$$